Mat. Res. Soc. Symp. Proc. Vol. 746 © 2003 Materials Research Society Q6.6

Magnetic Properties of Ni Nanoparticles Embedded in Amorphous SiO_2

Fabio C. Fonseca[1], Gerardo F. Goya[1], Renato F. Jardim[1], Reginaldo Muccillo[2], Neftalí L. V. Carreño[3], Elson Longo[3], Edson R. Leite[3]
[1] Instituto de Física, Universidade de São Paulo, CP 66318, 05315-970, São Paulo, SP, Brazil
[2] Centro Multidisciplinar de Desenvolvimento de Materiais Cerâmicos CMDMC, CCTM-Instituto de Pesquisas Energéticas e Nucleares, CP 11049, 05422-970, São Paulo, SP, Brazil
[3] Centro Multidisciplinar de Desenvolvimento de Materiais Cerâmicos CMDMC, Departamento de Química, Universidade Federal de São Carlos, CP 676, 13560-905, São Carlos, SP, Brazil

ABSTRACT

A modified sol-gel technique was used to synthesize nanocomposites of Ni:SiO_2 which resulted in Ni nanoparticles embedded in a SiO_2 amorphous matrix. Transmission electron microscopy TEM analysis were performed to study the structure and morphology of the magnetic powders. The Ni particles were found to have a good dispersion and a controlled particle size distribution, with average particle radius of ~ 3 nm. A detailed characterization of the magnetic properties was done through magnetization measurements M(T,H) in applied magnetic fields up to ± 7 T and for temperatures ranging from 2 to 300 K. The superparamagnetic (SPM) behavior of these metallic nanoparticles was inferred from the temperature dependence of the magnetization. The blocking temperature T_B, as low as 20 K, was found to be dependent on Ni concentration, increasing with increasing Ni content. The SPM behavior above the blocking temperature T_B was confirmed by the collapse of M/M_S vs. H/T data in universal curves. These curves were fitted to a log-normal weighted Langevin function allowing us to determine the distribution of magnetic moments. Using the fitted magnetic moments and the Ni saturation magnetization, the radii of spherical particles were determined to be close to ~ 3 nm, in excellent agreement with TEM analysis. Also, magnetic hysteresis loops were found to be symmetric along the field axis with no shift via exchange bias, suggesting that Ni particles are free from an oxide layer. In addition, for the most diluted samples, the magnetic behavior of these Ni nanoparticles is in excellent agreement with the predictions of randomly oriented and noninteracting magnetic particles. This was confirmed by the temperature dependence of the coercivity field that obeys the relation $H_C(T) = H_{C0}\,[1-(T/T_B)^{1/2}]$ below T_B with H_{C0} ~ 780 Oe.

INTRODUCTION

Nanosized superparamagnetic (SPM) particles of ferromagnetic metals as Fe, Co, and Ni have been extensively studied because of both the richness of their physical properties and a wide range of potential applications like catalysts, high density magnetic recording media, ferrofluids, and medical diagnostics [1,2]. Although they are easily obtained, a major point is the processing method used to produce such nanomaterials. In particular, several methods have been used to prepare Ni nanoparticles (NP) like evaporation [3], sputtering [4], high-energy ball milling [5], ion exchange, [6] and sol-gel [7,8]. However, metallic NP exhibit two main

problems: the control of particles size and the formation of an oxide layer surrounding the metallic particles. The control of particles size distribution (SD) and average size strongly depends on the parameters of the preparation method. Besides the processing technique used, an approach to assemble and maintain a nanostructured material is to host the metallic NP in an inorganic and non-magnetic matrix. The development of nanocomposites, in which metallic particles are embedded in a matrix, typically silica, can provide an effective way of tailoring a uniform SD and to control the dispersion of ultrafine particles [9].
In addition, these SPM particles have a high reactivity because of the very high surface area to volume ratio and can be easily environmentally degraded. Thus, as result of the processing method, an oxide surface layer can be formed leading to a shell-core morphology where an antiferromagnetic (AFM) oxide layer surrounds the ferromagnetic (FM) metallic NP. Such a morphology influences the magnetic properties due to the exchange interaction between the FM and AFM phases.

In the present study we focus on the magnetic characterization of high quality specimens of Ni nanoparticles embedded in amorphous silica prepared through a modified sol-gel precursor. Several physical characterizations performed on diluted samples of Ni:SiO_2, with Ni concentrations of ~ 1.5 and 5 wt%, indicated that they have average radius close to 3 nm, exhibit superparamagnetism (SPM), and are free from an oxide NiO layer.

EXPERIMENTAL

Nanocomposites of Ni:SiO_2 were synthesized by a modified sol-gel method using as start materials tetraethylorthosilicate (TEOS), citric acid, and nickel nitrate ($Ni(NO_3)_2.6H_2O$. The citric acid was dissolved in ethanol and the TEOS and the nickel nitrate were added together and mixed for homogenization during 15 min at room temperature. A citric acid/metal (Si+Ni) ratio of 3:1 (in mol) was used. Ethylene glycol was added to the citrate solutions, at a mass ratio of 40:60 in relation to the citric acid, to promote the polyesterification. The resulting polymer was pyrolysed in N_2 atmosphere at different temperatures and times: typically at 500 °C for 2 h. During the pyrolysis, the burn out of the organic material results in a rich CO/CO_2 atmosphere which promotes the reduction of the Ni-citrate, resulting in nanometric Ni particles. Here we concentrate our discussion in two diluted samples with ~ 1.5 and 5 Ni wt% which are referred in the text as samples S1 and S2, respectively. Further details of the preparation method employed are described elsewhere [7]. The structure and morphology of the magnetic powder were examined by high-resolution transmission electron microscopy (TEM) and X-ray diffraction (XRD) analysis. Magnetization measurements M(T,H) in applied magnetic fields between ± 7 T and for temperatures ranging from 2 to 300 K, were performed in powders with a SQUID magnetometer.

RESULTS AND DISCUSSION

Figure 1 shows a Dark-Field (DF) TEM image of the S1 sample. It is observed that the Ni nanoparticles (bright spots in the photograph) are well dispersed in the amorphous matrix. DF-

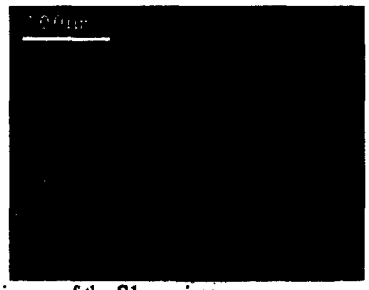

Figure 1. Dark-Field TEM image of the S1 specimen.

TEM analysis revealed that the Ni particles present an homogeneous particle SD, with a mean particle size of r_{mT} ~3.3 nm. The r_{mT} values are slightly higher but consistent with the average crystallite sizes determined from X-ray diffraction (XRD) data (not shown) through the Scherrer equation, as displayed in Table I. The particle SD's shown in Fig. 2 were built from TEM examinations by considering over than 400 particles. The log-normal SD's have distinct characteristics for the studied samples (Table I). For the sample S1, the median particle size r_{0T} = 3.9 nm is close to the mean particle size r_{mT} = 4.2 nm due to a small distribution width σ_T = 0.35 nm. The Ni richest sample S2 (not shown) revealed a SD with r_{0T} = 2.3 nm, r_{mT} = 3.3 nm, and a larger distribution width σ_T = 0.84 nm (see Table I).

Table I. Nanoparticles size distributions parameters[a].

Sample	log-normal L(x)					TEM analysis			XRD
	μ_0	r_0	μ_m	r_m	σ	r_{0T}	r_{mT}	σ_T	r_{XR}
S1	4.6	2.8	12	3.8	1.4	3.9	4.2	0.35	2.7
S2	5.1	2.9	17	4.4	1.6	2.3	3.3	0.84	2.3

[a]Magnetic moment values in emux 10^{17} and radii in nm.

The magnetic properties of these nanocomposites are also of interest. The temperature dependence of the magnetization M(T), taken in zero-field-cooling (ZFC) and field-cooling (FC) conditions, exhibits clear features of SPM systems. These features are displayed in Figure 3 for both samples: (1) the ZFC curves are rounded at T_B, defined as the temperature of their maximum, indicating a blocking process of the small particles; and (2) a paramagnetic-like behavior above T_B. The value of T_B shifts from $T_B \approx 20$ K for the S1 sample to $T_B \approx 40$ K for the more concentrated S2 sample. This shift of T_B to higher temperatures is consistent with a higher metal content in sample S2.

Further evidence of the SPM behavior above T_B was inferred from hysteresis loops shown in the inset of Fig. 3. The M/M_S vs. H/T data, for $T > T_B$, resulted in a universal curve, a feature of the SPM response [10]. The magnetic moment distributions were fitted considering a log-normal weighted Langevin function (log-normal L(x)) [10]. From these fittings, the radius distributions of spherical particles were calculated using the saturation magnetization of bulk Ni at 300 K (M_S = 521 emu/cm^3). The mean radii r_m were estimated to be 3.8 and 4.4 nm for samples S1 and S2, respectively, in excellent agreement with the ones obtained from TEM analyses.

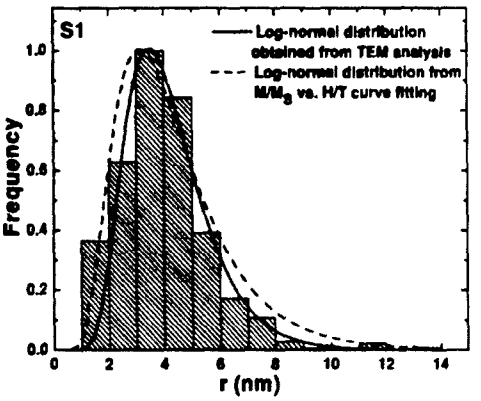

Figure 2. Histogram of the size distribution of Ni nanoparticles and log-normal fitting (solid line) for sample S1 determined from TEM analysis. Dashed line stands for the log-normal size distribution calculated from the log-normal Langevin L(x) fitting for M/M_S vs. H/T curves (see text for details).

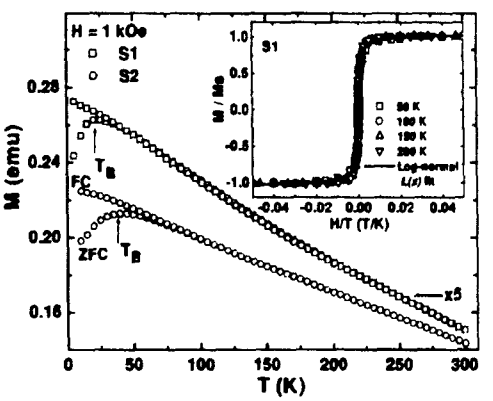

Figure 3. Temperature dependence of the magnetization for samples S1 and S2. Curves were taken in ZFC and FC processes at H = 1 kOe. The inset shows a universal M/M_S vs. H/T curve of the S1 specimen, for several temperatures.

A comparison between the log-normal SD's inferred by either TEM analysis and magnetic-data fitting for the more diluted sample S1 is shown in Fig. 2. The excellent agreement between the two log-normal SD's lends credence to our analysis and may be attributed to both a narrow SD and a negligible interaction between particles [10]. The same analysis, for the more concentrated specimen S2 (not shown) resulted in a poorer agreement, with r_0 being slightly higher than r_{0T} but close to r_{mT} (see Table I). Such a small discrepancy is certainly related to either a magnetic contribution arising from larger particles and weak dipolar interactions [10].

Turning now to the low temperature regime, Fig. 4 shows the hysteresis loops measured

at temperatures ranging from 3.5 to 200 K for sample S1. We remark that NiO/Ni composites exhibit exchange bias due to interfacial interaction between ferromagnetic Ni and antiferromagnetic AFM NiO [11]. This exchange interaction is evidenced through a shift of hysteresis loops along the field axis when the system is field-cooled below the ordering temperature of the AFM phase. Defining $H_{C}+$ and $H_{C}-$ as the coercive fields with decreasing and increasing fields, respectively, a measure of the symmetry of the M(H) curves is given by $\Delta H_C = (H_{C}+ + H_{C}-)/2$. Previous works on Ni/NiO systems have reported values for the exchange bias field ΔH_C ranging from ~ 80 Oe in Ni/NiO nanowires [12], to ~ 700 Oe in partially oxidized Ni NP [13]. The hysteresis loops displayed in Fig. 4 clearly show that these loops are symmetric about zero field (ΔH_C ~ 1 Oe) indicating the absence of particles with the shell-core NiO-Ni morphology. The data also indicate negligible contribution of isolated NiO nanoparticles, which would exhibit large loop shifts of up to ~ 10 kOe [14]. Thus, our magnetic data strongly suggest that the modified sol-gel method used for the synthesis of nanosized Ni metallic particles results in significantly less oxidized metallic particles than other techniques [12,13]. This result is in agreement with XRD analysis which revealed absence of extra phases in these samples.

The $H_C(T)$ values at different temperatures (Figure 4 (b)) reveal that coercivity develops appreciably below T_B in these samples. The coercivity for a system of randomly oriented and noninteracting particles is expected to follow the relation $H_C(T) = H_{C0}\,[1-(T/T_B)^{1/2}]$ with $H_{C0} = 0.64K/M_S$ [15], where K is the anisotropy constant of bulk Ni, and M_S is the saturation magnetization. The above expression considers that the magnetization reversal takes place coherently, a situation that can be achieved when interparticle interactions are neglected [16]. Figure 4 (b) shows that this dependence is closely followed by both samples, supporting the picture of noninteracting particles, as previously observed in systems comprised of metallic and ferromagnetic NP [17]. Also, the extrapolation of $H_C(T)$ to 0 yields values of T_B ~ 16 and 27 K for samples S1 and S2, respectively, consistent with those obtained from M(T) curves.

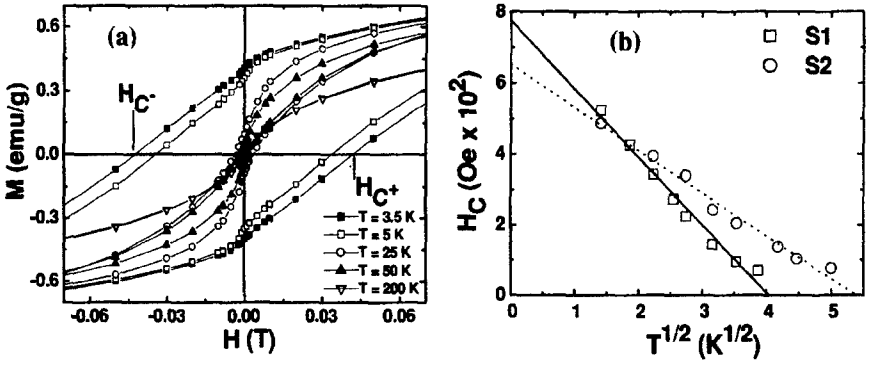

Figure 4. (a) Expanded view of hysteresis loops taken at 3.5, 5, 25, 50, and 200 K for the nanocrystalline Ni particles sample S1. $H_{C}+$ and $H_{C}-$ are defined in the text. (b) Temperature dependence of the coercivity H_C for samples S1 and S2. The Figure shows $H_C(T)$ to obey a $T^{1/2}$ dependence with H_{C0} of ~ 780 and 650 Oe for samples S1 and S2, respectively.

CONCLUSIONS

In summary, a modified sol-gel method to prepare high-quality Ni:SiO_2 nanocomposites has been developed. The obtained Ni-NP have mean radius of ~ 3 nm, narrow particle SD's, and exhibit SPM behavior above T_B ($T_B < 40$ K). The Ni-NP size distributions, determined from magnetic measurements, were in excellent agreement with those obtained from TEM analysis. Due to the absence of a shift along the field axis in M(H) curves below T_B and XRD data, we have also inferred that these Ni-NP are free from an oxide layer. The linear $T^{1/2}$ dependence of the coercivity bellow T_B supports a picture of randomly oriented and noninteracting ferromagnetic nanoparticles in the samples studied.

ACKNOWLEDGMENTS

We are grateful to A. L. Brandl, J. Cesar, and M. Knobel for the program codes for distribution calculations. This work was supported in part by the Brazilian agency FAPESP under Grant Nos. 99/10798-0, 01/02598-3, 98/14324-0, and 01/04231-0. Three of us (R.F.J., G.F.G., and E.R.L.) are fellows of the CNPq.

REFERENCES

1. M. Ozaki, *Mater. Res. Bull.* XIV, 35 (1989).
2. H. Gleiter, *Nanostruct. Mater.* **1**, 1 (1992).
3. T. Hayashi, T. Ohno, S. Yatsuya, R. Ueda, *Jap. J. Appl. Phys.* **16**, 705 (1977).
4. A. Gavrin, C. L. Chien, *J. Appl. Phys.* **73**, 6949 (1993).
5. E. M. González, M. I. Montero, F. Cebollada, C. de Julián, J. L. Vicent, J. M. González, *Europhys. Lett.* **42**, 91 (1998).
6. J. S. Jung, W. S. Chae, R. A. McIntyre, C. T. Seip, J. B. Wiley, C. J. O'Connor, *Mater. Res. Bull.* **34**, 1353 (1999).
7. E. R. Leite, N. L. V. Carreño, E. Longo, A. Valentini, and L. F. D. Probst, *J. Nanosci. Nanotechnol.* **2**, 89 (2002).
8. C. Estournès, T. Lutz, J. Happich, T. Quaranta, P. Wissler, J. L. Guille, *J. Magn. Magn. Mater.* **173**, 83 (1997).
9. C. A. Morris, M. L. Anderson, R. M. Stroud, C. I. Merzbacher, and D. R. Rolison, *Science* **284**, 622 (1999).
10. F. C. Fonseca, G. F. Goya, R. F. Jardim, R. Muccillo, N. L. V. Carreño, E. Longo, and E. R. Leite, *Phys. Rev. B* **66**, 104406 (2002).
11. J. B. D. Cullity, *Introduction to magnetic materials* (Addison-Wesley, Reading, Mass., 1972) Chap. 11.
12. M. Fraune, U. Rudiger, G. Guntherodt, S. Cardoso, and P. Freitas, *Appl. Phys. Lett.* **77**, 3815 (2001).
13. Y. D. Yao, Y. Y. Chen, M. F. Tai, D. H. Wang, and H. M. Lin, *Mater. Sci. Eng.* **A217**, 837 (1996).
14. R. H. Kodama, S. A. Makhlouf, and A. E. Berkowitz, *Phys. Rev. Lett.* **79**, 1393 (1997).
15. R. M. Bozorth, *Ferromagnetism* (Van Nostrand, Princenton, N. J., 1956) Chap. 18, pag. 831.
16. E. C. Stoner and E. P. Wohlfarth, *Trans. Roy. Soc.* (London) **A240**, 599 (1948).
17. M. E. McHenry, S. A. Majetich, J. O. Artman, M. DeGraef, and S. W. Staley, *Phys. Rev. B* **49**, 11358 (1994).